Journal of Materials Chemistry A

Accepted Manuscript

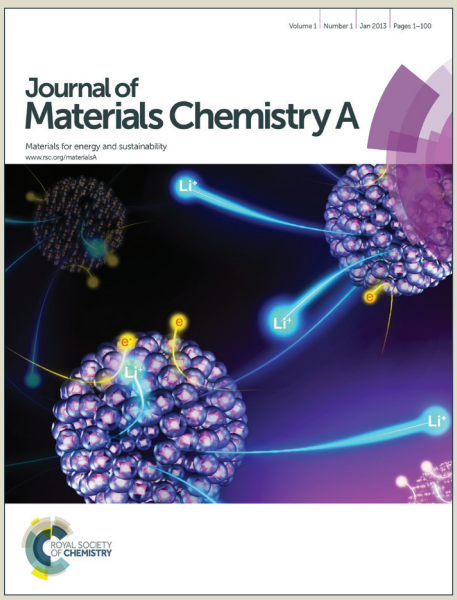

ROYAL SOCIETY OF CHEMISTRY

www.rsc.org/materialsA

Side-Chain Engineering of Benzodithiophene-Thiophene Copolymers with Conjugated Side Chain Containing Electron-Withdrawing Ethylrhodanine Group

Lixia Chen,[a,b] Ping Shen,[*a] Zhi-Guo Zhang,[b] Yongfang Li[*b]

[a] *College of Chemistry and Key Laboratory of Environmentally Friendly Chemistry and Applications of Ministry of Education, Xiangtan University, Xiangtan 411105, China*

[b] *Beijing National Laboratory for Molecular Sciences, CAS Key Laboratory of Organic Solids, Institute of Chemistry, Chinese Academy of Sciences, Beijing 100190, China*

*Correspondence to: E-mail: shenping802002@163.com (P. Shen); liyf@iccas.ac.cn (Y. Li)

ABSTRACT

Four benzodithiophene (BDT)-thiophene (T) copolymers with conjugated side chain containing electron-withdrawing ethylrhodanine acceptor unit, **PHDBDT-T-R**, **PEHBDT-T-R**, **PHDBDT-T-TR**, and **PEHBDT-T-TR,** were designed and synthesized for investigating the effect of side chains on the physicochemical properties and photovoltaic performance of the conjugated polymers. All the four copolymers possess an identical conjugated backbone of alternative benzodithiophene-thiophene, but different side chains on BDT and thiophene units, respectively. Polymer solar cells (PSCs) with these polymers as donor and $PC_{70}BM$ as acceptor exhibit an initial power conversion efficiency (PCE) of 0.61% for **PHDBDT-T-R**, 2.32% for **PEHBDT-T-R**, 1.46% for **PHDBDT-T-TR**, and 2.36% for **PEHBDT-T-TR**. After the treatment with 3 vol % DIO additive and with methanol, the highest PCE was increased up to 1.01%, 4.04%, 3.47%, and 4.25% for

PHDBDT-T-R, **PEHBDT-T-R**, **PHDBDT-T-TR**, and **PEHBDT-T-TR**, respectively, with significantly increased J_{sc} and FF. The effects of methanol treatment on the photovoltaic performance of the PSCs can be ascribed to the increased carrier transport, improved exciton dissociation and optimized phase separation of the active layer. This work indicates that side-chain engineering plays a key role on molecular structures and optoelectronic properties.

KEYWORDS: Polymer solar cells, Side-chain engineering, Ethylrhodanine, Photovoltaic properties

Introduction

Solar energy as a green energy resource has attracted great attention. Polymer solar cell (PSC) has been developed rapidly in recent years owing to its advantages of low cost, light weight, easy fabrication and capability to be fabricated into large area flexible devices.[1-5] The most successful PSCs to date are the devices based on the bulk heterojunction (BHJ) blend active layer of conjugated polymer electron donor and fullerene derivative electron acceptor (such as [6,6]-phenyl-C_{61}-butyric acid methyl ester ($PC_{60}BM$) and [6,6]-phenyl-C_{71}-butyric acid methyl ester ($PC_{70}BM$)).[6] The priority in the studies of PSCs is how to increase the power conversion efficiency (PCE) of the devices. The PCE is proportional to the values of short-circuit current density (J_{sc}), open-circuit voltage (V_{oc}), and fill factor (FF) of the PSC. The J_{sc} depends on the efficiencies of the light absorption of the active layer, exciton diffusion to and dissociation at the D/A interface, charge transportation in the active layer, and charge collection on the electrodes. V_{oc} is mainly proportional to the difference between the lowest unoccupied molecular orbital (LUMO) energy level of the acceptor (e.g. $PC_{70}BM$) and the highest occupied molecular orbital (HOMO) energy level of the polymer donor. FF is related to the charge carrier mobilities and device fabrication conditions. While in order to increase the PCE of the PSCs, it is very important to design and synthesize new conjugated polymer donors with narrower bandgap (broader absorption) for higher J_{sc}, relatively lower-lying HOMO

energy level for higher V_{oc}, and higher hole mobility for higher J_{sc} and larger FF.

Among high performance conjugated donor-acceptor (D-A) polymer photovoltaic materials, benzo[1,2-*b*:4,5-*b*']dithiophene (BDT) has been widely investigated and used as a donor unit due to its good electron-donating properties, rigid coplanar structure with stronger π-π intermolecular interactions, and the possibility of side chain manipulation for suitable solubility and processability.[7-9] 3-Ethylrhodanine is a dye unit, usually used as an electron-withdrawing group, which could greatly improve the light absorption ability, and thus, a high J_{sc} value could be achieved in the corresponding photovoltaic devices.[10]

Equally important is that some studies have been directed towards understanding of the effects of side chains on the photovoltaic performance of PSCs based on D-A copolymers. Recent work suggests that for the same conjugated polymer backbone the type (alkyl, alkoxy, aryl), shape, topology (linear, branched) and distribution (uniform, alternating, random) of side chains have a large impact on the morphology (crystallinity, π-stacking orientations), charge transport and photovoltaic properties of the polymers.[11-17] Thus the side chain effect should also be fully explored in the design of new copolymers for highly efficient solar cells. In previous work, our group have reported some side chain engineering of the BDT-bithiazole-based D-A copolymers, a PCE of 3.71% was achieved in combination with $PC_{70}BM$ acceptor.[11] It is worth mentioning that high PCEs of 8-10% were achieved just by the side chains engineering of a BDT-T-S and thieno[3,4-b]thiophene copolymers.[8,17,18]

On the basis of the above consideration, we herein designed and synthesized four main chain-side chain D-A polymers (**PHDBDT-T-R**, **PEHBDT-T-R**, **PHDBDT-T-TR**, and **PEHBDT-T-TR**, Fig. 1) based on BDT and thiophene with alkoxy side chain onto the BDT unit and end-capping ethylrhodanine group as an electro-withdrawing conjugated side chain on thiophene unit. For the four polymers, we chose 2-hexlydecyloxy (HD) and 2-ethylhexyloxy (EH) as side chains on BDT unit to systematically investigate the effects of side chain shape and size (EH vs. HD) on solubility, light absorption, HOMO/LUMO energy levels, and charge transport properties of the resulting polymers as well as on morphology and photovoltaic

properties of the PSCs. On the other hand, the inserted thienylvinyl between thiophene and end-capping 3-ethylrhodanine group gives a chance to study the influence of the extended conjugated side chain on optoelectronic properties of the copolymers.

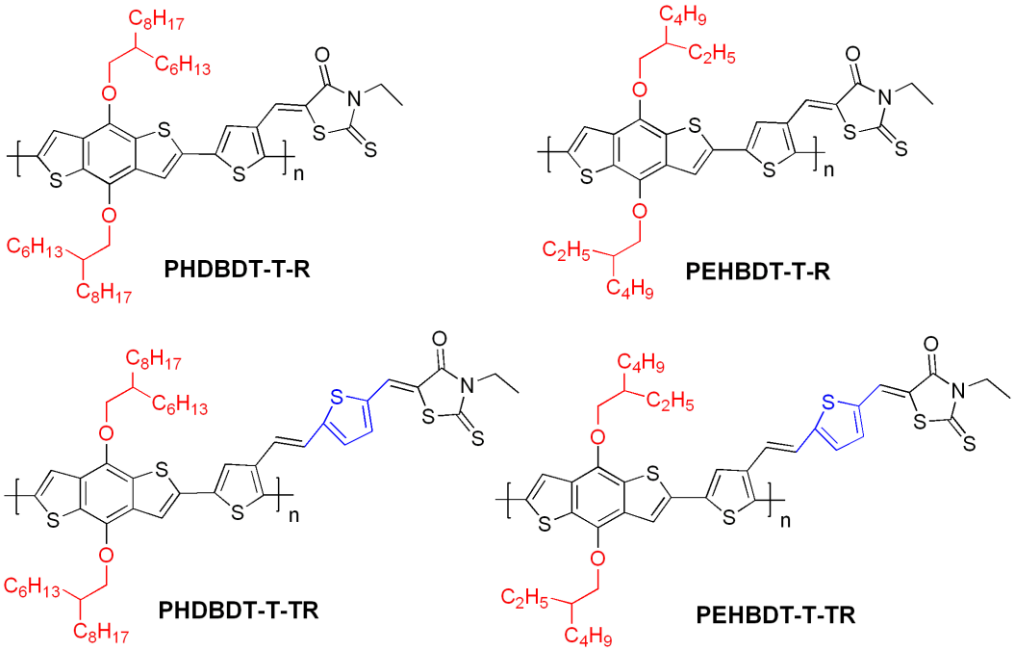

Fig. 1 Chemical structures of the four copolymers.

Results and discussion

Synthesis and characterization

The chemical structures and synthesis routes of monomers and the four polymers are outlined in Fig. 1 and Scheme 1, respectively. **PHDBDT-T-R**, **PEHBDT-T-R**, **PHDBDT-T-TR**, and **PEHBDT-T-TR** have an identical BDT-thiophene copolymer backbone but different side chains attached on BDT and thiophene units. **PEHBDT-T-R** and **PEHBDT-T-TR** have ethylhexyloxyl side chains, **PHDBDT-T-R** and **PHDBDT-T-TR** have more branched hexyloctyloxyl side chains attached on BDT unit to further improve solubility of the resulting polymers (Fig. 1). 3-Ethylrhodanine was chosen as an end-capping side chain to build these main chain-side chain type D-A copolymers due to its intrinsic electron-deficient character. Compared with **PEHBDT-T-R** and **PHDBDT-T-R**, **PEHBDT-T-TR** and **PHDBDT-T-TR** possess extended conjugated side chains with the aim to red-shift

absorption spectra and lower bandgaps of the polymers. The choice of these different side chains is convenient for fine-tuning of the optoelectronic properties of the resulting polymers.

As outlined in Scheme 1, two monomers **M3** and **M4** based on BDT unit were prepared according to the procedure in the literature.[19] Compound **1** was synthesized by the bromination reaction of thiophene-3-carbaldehyde. Then thiophene-based monomer **M1** containing 3-ethylrhodanine moiety was synthesized by the Knoevenagel reaction between Compound **1** and 3-ethylrhodanine. Monomer **M2** with an extended thienylvinyl moiety was synthesized via the stepwise synthetic protocol. First, compound **2** was synthesized according to published procedures.[20] Next this compound was converted into compound **3** via Vilsmeier reaction. Monomer **M2** was subsequently obtained by the Knoevenagel reaction like the **M1**. Compounds **1**-**3** and **M1**, **M2** were satisfactorily characterized by ^{1}H NMR and EI or MALDI-TOF spectroscopies. Four new D-A copolymers were synthesized successfully via Stille-type copolymerization of a distannane monomer (**M3** or **M4**) with 3-ethylrhodanine-based monomers **M1** and **M2**. Table 1 summarized the polymerization results and thermal properties of the copolymers.

The polymers can be readily dissolved in common organic solvents, such as chloroform, tetrahydrofuran (THF), chlorobenzene, and 1, 2-dichlorobenzene (DCB) at room temperature or with a slightly heating. The molecular weight and polydispersity (PDI) values of the four polymers was measured by the GPC method (against polystyrene standards) in chloroform at room temperature (Table 1). Among the four copolymers, **PHDBDT-T-R** gives the lowest weight-average molecular weight (M_w) of 17.7 kDa with a PDI of 1.86 (Table 1), whereas **PEHBDT-T-R** shows the highest M_w of 50.8 kDa with a moderate PDI of 2.68 (Table 1). **PHDBDT-T-TR** and **PEHBDT-T-TR** have the moderate M_w of 39.5 kDa and 25.2 kDa, respectively.

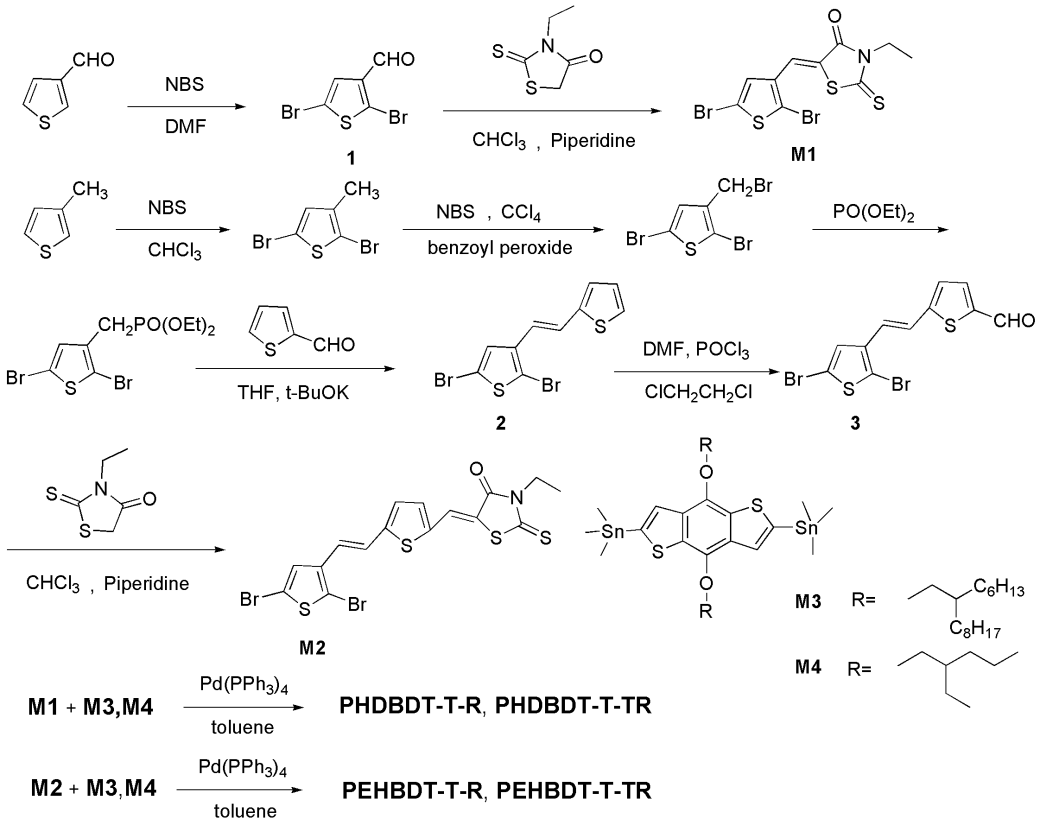

Scheme 1 Synthetic routes of the monomers and the four copolymers.

The thermal stability of conjugated polymers is very important for their application in optoelectronic device. The thermal properties of the polymers were investigated with thermogravimetric analysis (TGA) measurement. The four polymers have good thermal stability with onset decomposition temperatures corresponding to 5% weight loss (T_d) at above 290 ℃, as shown in Table 1 and Fig. 2. **PHDBDT-T-R** and **PEHBDT-T-R** show relatively high T_d of 327 ℃ and 329 ℃, respectively (Fig. 2), which are higher than those of **PHDBDT-T-TR** (316 ℃) and **PEHBDT-T-TR** (299 ℃). The results suggest that the absence of a thienylvinyl moiety between the thiophene and 3-ethylrhodanine as conjugated side chains benefits to improve the thermal stability of the resulting polymers. Obviously, the thermal stability of the polymers is adequate for the applications in PSCs and other optoelectronic devices.

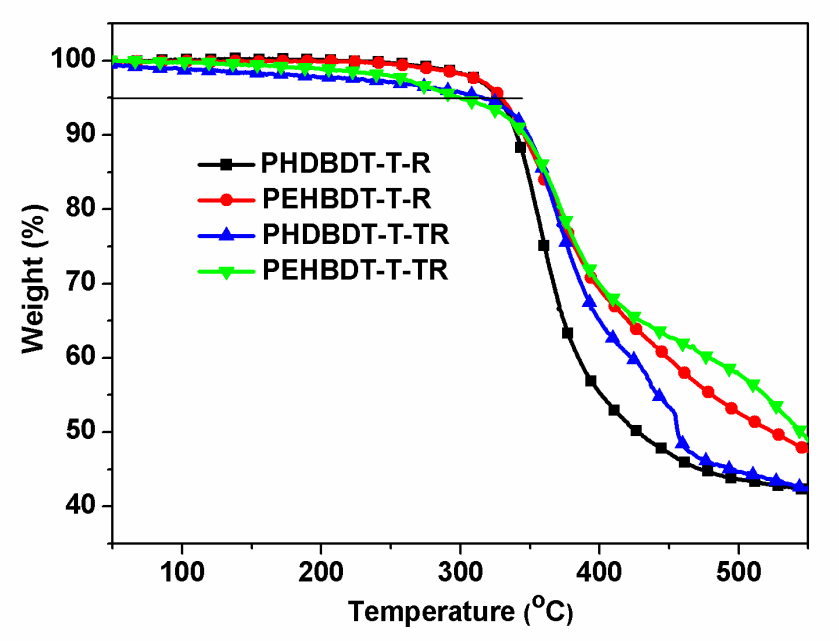

Fig. 2 TGA plots of **PHDBDT-T-R**, **PEHBDT-T-R**, **PHDBDT-T-TR** and **PEHBDT-T-TR** with a heating rate of 10 ℃/min under an inert atmosphere.

Table 1 Molecular weights and thermal properties of the synthesized copolymers

polymer	Yield (%)	M_n (kDa)[a]	M_w (kDa)[a]	PDI	T_d (°C)[b]
PHDBDT-T-R	41.6	9.5	17.7	1.86	327
PEHBDT-T-R	78.3	18.9	50.8	2.68	329
PHDBDT-T-TR	51.1	13.8	25.2	1.82	316
PEHBDT-T-TR	72.6	11.6	39.5	3.41	299

[a] Determined by GPC in $CHCl_3$ based on polystyrene standards. [b] Decomposition temperature, determined by TGA in nitrogen, based on 5% weight loss.

Optical properties

Optical properties of these polymers have been investigated by UV-vis absorption spectroscopy in dilute chloroform solution and as thin solid films (Fig. 3). The detailed absorption data including the absorption maximum wavelength (λ_{max}) in both solution and films, the absorption edge (onset wavelength of the absorption peak, λ_{edge}) of the polymer films, and optical bandgaps (E_g^{opt}) are summarized in Table 2. As shown in Fig. 3a, in solution **PEHBDT-T-R** exhibits two distinct absorption bands. The first absorption band with a λ_{max} at 435 nm, is assigned to the delocalized excitonic π-π* transition. The second absorption band located at longer wavelength

range with a λ_{max} at 538 nm, can be attributed to an intramolecular charge transfer (ICT) states between main-chain donor and side-chain acceptor.[21] As for **PHDBDT-T-R**, it shows a similar absorption shape to **PEHBDT-T-R** except for a shoulder peak at the longer wavelength range. In comparison with **PHDBDT-T-R** and **PEHBDT-T-R**, **PHDBDT-T-TR** and **PEHBDT-T-TR** with extended side chains have just one broad absorption band ranged from 300 to 700 nm with λ_{max} of 471 and 475 nm, respectively. This should be ascribed to that the introduction of a thienylvinyl moiety between thiophene and 3-ethylrhodanine weakens the ICT absorption between the main-chain donor and side-chain acceptor. The weakened ICT absorption lead to a blue-shifted ICT band, which overlaps with π-π* transition absorption band and finally exhibits one broad absorption band. Compared to the absorption spectra of the polymer solutions, the absorption spectra of the films are broadened and the λ_{max} values are red-shifted (Fig. 3b). This phenomenon results from the enhanced interchain interaction in the solid films, which may be related to the increased extent of π-π* stacking of the backbones and increased polarizability of the film, or both.[22] The absorption edge (λ_{edge}) of **PEHBDT-T-R** and **PEHBDT-T-TR** film are ~20 nm red-shifted than those of the **PHDBDT-T-R** and **PHDBDT-T-TR** film, respectively. The optical bandgaps (E_g^{opt}) of **PHDBDT-T-R**, **PEHBDT-T-R**, **PHDBDT-T-TR**, and **PEHBDT-T-TR** are 1.92, 1.86, 1.90, and 1.84 eV, respectively, calculated from λ_{edge} of their solid state films (Table 2). Obviously, the polymers with EH as a side chain possess lower bandgaps than those of HD as a side chain. It may be due to that the more branched HD side chain on BDT unit damaged the coplanarity of the main chain. On the other hand, the result showed that the extended conjugated side chains attached onto thiophene unit can red-shift the absorption edges and lower bandgaps, which is favorable to improve the J_{sc} of PSCs based on these polymers (e.g. **PHDBDT-T-R** vs **PHDBDT-T-TR** and **PEHBDT-T-R** vs **PEHBDT-T-TR**) as donor.

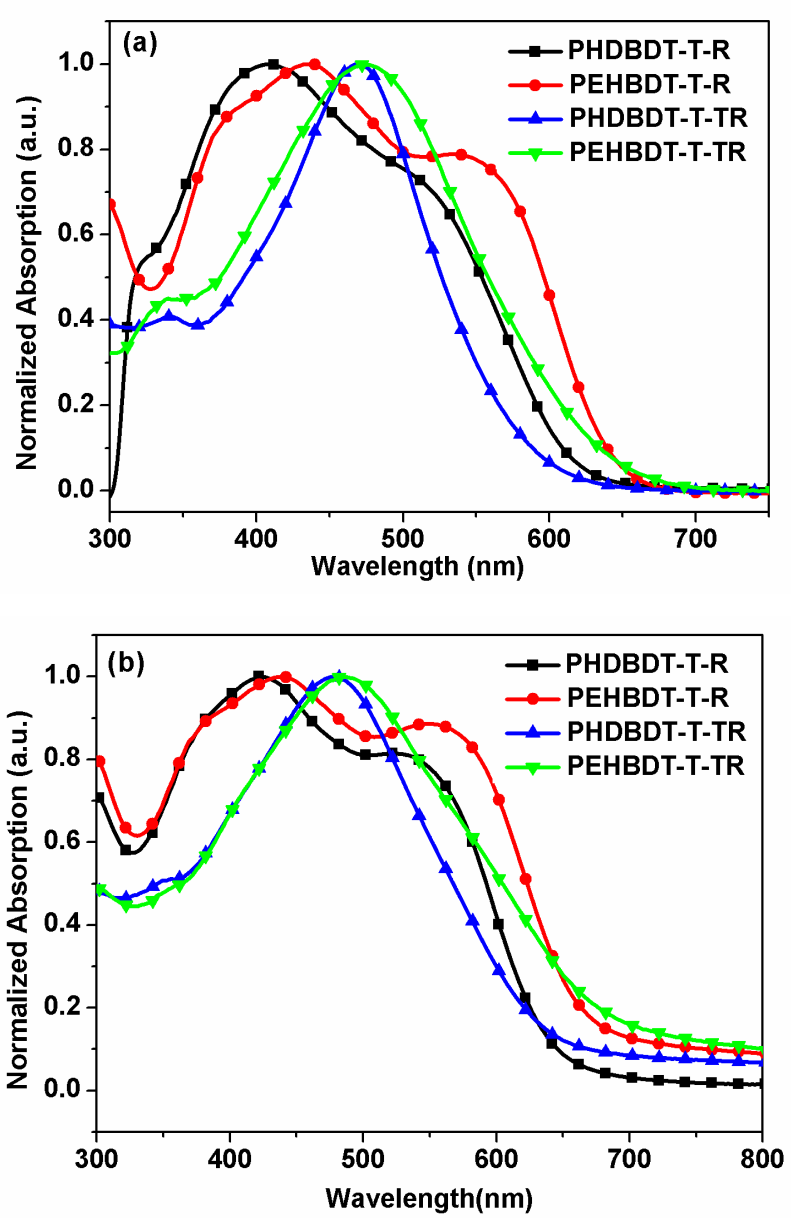

Fig. 3 Normalized absorption spectra of **PHDBDT-T-R**, **PEHBDT-T-R**, **PHDBDT-T-TR** and **PEHBDT-T-TR** in (a) chloroform solution and (b) thin film on quartz.

Electrochemical properties

Cyclic voltammetry (CV) was employed to measure the electronic energy levels of conjugated polymers. The HOMO and LUMO energy levels of conjugated polymers are crucial for the application as photovoltaic materials in PSCs, which can be estimated from the onset oxidation and reduction potentials ($E_{ox/red}$) in the voltammograms. The CV of the four polymer films were measured on a Pt electrode

in a 0.1 mol/L Bu_4NPF_6-acetonitrile solution (Fig. 4). The results of the electrochemical properties are also summarized in Table 2. The CV curve was recorded by using an Ag/AgCl electrode as a reference, which was calibrated against the redox potential of ferrocene/ferrocenium couple (Fc/Fc^+ measured as 0.39 V vs Ag/AgCl), whose energy level was assumed to be 4.80 eV below the vacuum level. Thus, HOMO/LUMO = $-e(E_{ox/red} + 4.41)$ (eV), where $E_{ox/red}$ is the oxidation/reduction onset potential of the sample vs Ag/AgCl.

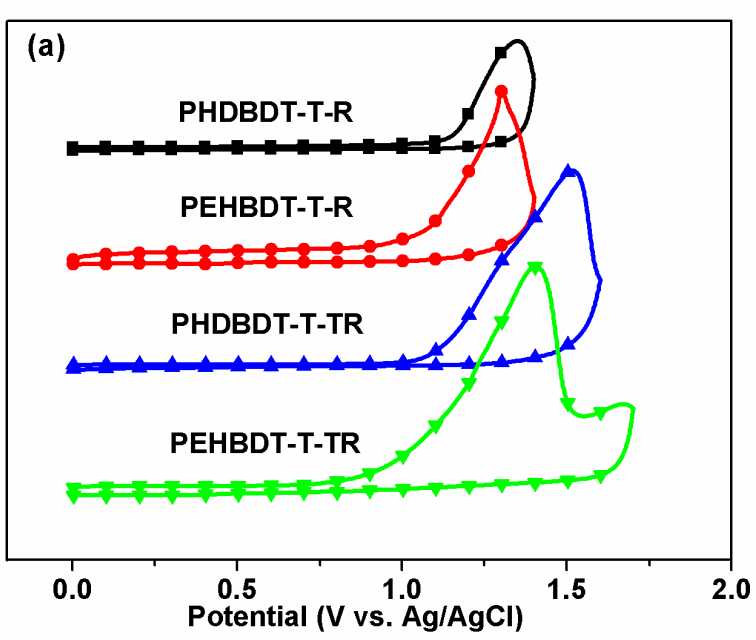

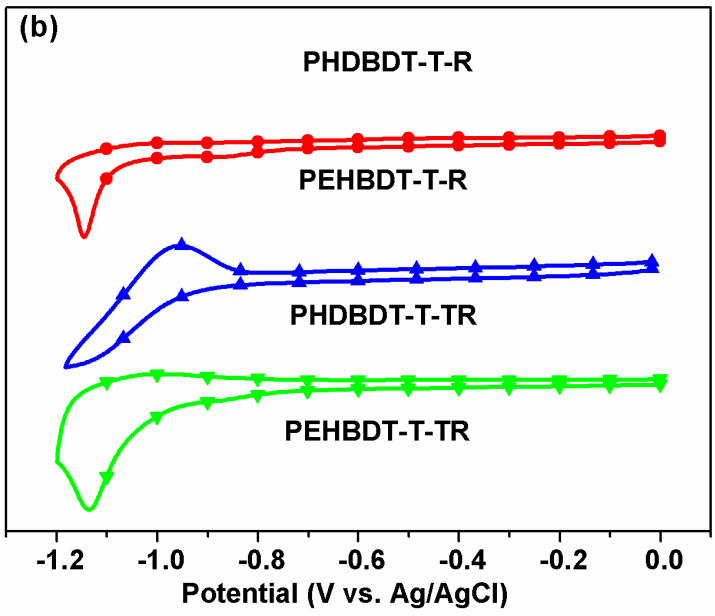

Fig. 4 Cyclic voltammograms of the polymer films on platinum electrode in

acetonitrile solution containing 0.1 mol L^{-1} Bu_4NPF_6 at a scan rate of 0.1 V s^{-1}, (a) the oxidation segments, (b) the reduction segments.

Table 2 Optical and electrochemical properties of the four copolymers

Polymer	λ_{max} [a] (nm)	λ_{max} [b] (nm)	λ_{edge} [c] (nm)	E_g^{opt} [d] (eV)	E_{ox}/HOMO [e] (V/eV)	E_{red}/LUMO [e] (V/eV)
PHDBDT-T-R	407,511	424,530	645	1.92	1.15/-5.56	-1.02/-3.39
PEHBDT-T-R	435, 538	440, 552	665	1.86	1.07/-5.48	-1.08/-3.33
PHDBDT-T-TR	471	478	652	1.90	1.10/-5.51	-0.95/-3.46
PEHBDT-T-TR	475	488	673	1.84	1.04/-5.45	-1.03/-3.38

[a]Measured in dilute chloroform solution. [b]Measured on quartz plate by polymers cast from chloroform solution. [c]Absorption edge of the thin films. [d]Estimated from the onset wavelength of the absorption spectra: $E_g^{opt} = 1240/\lambda_{edge}$. [e]Calculated according to the equation: HOMO/LUMO = −e ($E_{ox/red}$ + 4.41) (eV).

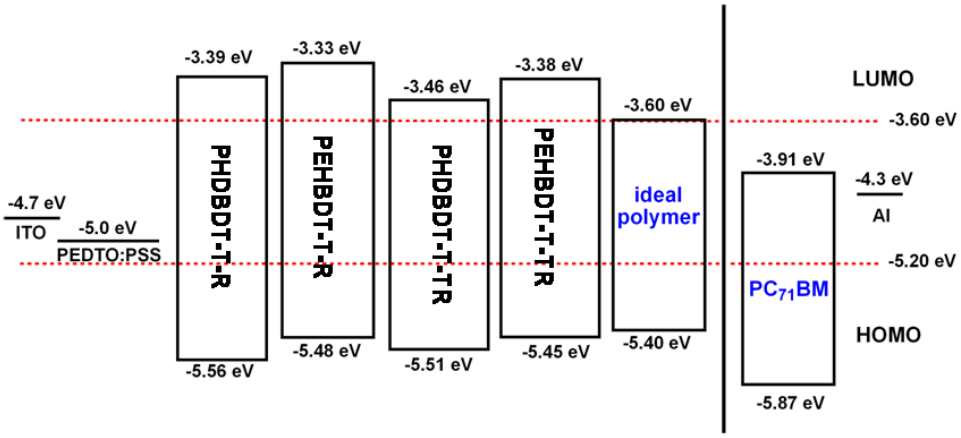

Fig. 5 Energy level diagrams for the four polymers, ideal polymer and $PC_{70}BM$. The dashed lines indicate the thresholds for air stability (-5.20 eV) and effective charge transfer to $PC_{70}BM$ (-3.91 eV).

On the other hand, the onset reduction potential (E_{red}) values are observed as -1.02, -1.08, -0.95, and -1.03 V vs Ag/AgCl for **PHDBDT-T-R**, **PEHBDT-T-R**, **PHDBDT-T-TR**, and **PEHBDT-T-TR**, respectively (Fig. 4b). Accordingly, the calculated LUMO energy levels of the polymers are -3.39, -3.33, -3.46, and -3.38 eV, respectively. Evidently, the different side chains both on BDT and thiophene units have some effects on the LOMO energy levels of the resulting polymers. Moreover, the LUMO energy levels of the polymers are all located within a suitable range and

are much higher than that of $PC_{70}BM$ (ca. -3.91 eV),[25] thus, efficient exciton dissociation could be expected to occur in their corresponding PSCs. A complete picture of the energy levels and band structure of the four polymers and $PC_{70}BM$ is presented in Fig. 5. As can be seen from the Fig. 5, both the HOMO and LUMO energy levels of the copolymers are close to the ideal range.

Photovoltaic properties

To investigate the effects of different side chains on the photovoltaic properties of the BDT–thiophene-based copolymers, bulk heterojunction PSC devices with a configuration of ITO/PEDOT:PSS/polymer:PCBM/Ca/Al was fabricated. The active layers were spin-coated from DCB solution of polymer:$PC_{70}BM$ blend. The thickness of the active layer was controlled by changing the spin speed during the spin-coating process and measured on an Ambios Tech. XP-2 profilometer. The corresponding open-circuit voltage (V_{oc}), short-circuit current (J_{sc}), fill factor (FF), and power conversion efficiency (PCE) of the devices are summarized in Table 3. Fig. 6 shows the typical current density–voltage curves (*J*–*V*) of the PSCs based on the blends of polymer:$PC_{70}BM$ under the illumination of AM1.5G, 100 mW/cm^2 and Fig. 7 shows the external quantum efficiency (EQE) curves of the PSCs.

First, the blend ratio of the polymer donor and $PC_{70}BM$ acceptor was optimized. For example, when the mixing ratio of **PHDBDT-T-R** and $PC_{70}BM$ increased from 1: 1 to 1:2 to 1:3, the PCE of the device continuously increased from 0.17% to 0.25% to 0.61% (Table 3). It can be observed that an increase in the $PC_{70}BM$ content resulted in a slight increase in the V_{oc} and also elevated the J_{sc} and FF. It is obvious that the optimal blend ratio for this polymer was determined to be around 1:3. The blend ratio of the other three polymers was also optimized. It is found that the different polymers have their own optimal blend ratio and the determined optimal blend ratios are 1:2, 1:2 and 1:1.5, for **PEHBDT-T-R**, **PHDBDT-T-TR** and **PEHBDT-T-TR**, respectively. On each optimal blend ratio, the best PCE of the four polymers are 0.61%, 2.32%, 1.46% and 2.36%, respectively.

Next, we investigated the effect of the high boiling point additive 1,

8-diiodooctane (DIO) on the photovoltaic properties of the copolymers (Table 3). Except for **PHDBDT-T-R**, the other three polymers achieve improved PCEs. For example, the V_{oc}, J_{sc} and FF values of **PEHBDT-T-R** were improved significantly, when a small amount of DIO (3%, by volume) was added, resulting in remarkably improvement of PCE (Table 3). While when 3 vol % DIO was added to **PEHBDT-T-TR** based cell, J_{sc} value was improved, V_{oc} and FF values remain unchanged. In these optimized conditions, the maximal PCEs of 3.31% (V_{oc} = 0.87 V, J_{sc} = 7.79 mA/cm^2, FF = 48.89%), 1.64% (V_{oc} = 0.93 V, J_{sc} = 3.89 mA/cm^2, FF = 45.33%) and 2.80% (V_{oc} = 0.69 V, J_{sc} = 8.79 mA/cm^2, FF = 46.20%) are achieved for the **PEHBDT-T-R**, **PHDBDT-T-TR** and **PEHBDT-T-TR** based devices (Table 3). Inspired by recent work[26-31] on post solvent treatment, we tried to employ a polar solvent methanol to further optimize the photovoltaic performance of PSCs. From Table 3 and Fig. 6, one can see that the photovoltaic performance of all the copolymers had been enhanced after the solvent treatment. For instance, the PCE of **PEHBDT-T-TR** is further improved up to 4.25% with an increased V_{oc} from 0.69 V to 0.87 V, a J_{sc} from 8.79 mA/cm^2 to 9.36 mA/cm^2, and a FF from 46.20% to 52.30%. The improved efficiency may originate from enhanced charge transport, or improved efficiency of carrier collection, which result from the creation of an optimal morphology under the conditions of DIO as the processing additive and treated with methanol. This is supported by results of the hole mobility measurements, morphology studies, photoluminescence (PL) quenching (vide infra). The highest PCE of 4.04% for **PEHBDT-T-R** with a small alkyl chain (EH) on BDT is significantly higher than that of the analogy polymer **PHDBDT-T-R** (1.01%) with a relatively bulky alkyl chain (HD) on BDT, as the same, the highest PCE of **PEHBDT-T-TR** (4.25%) is higher than **PHDBDT-T-TR** (3.47%). The results indicate that the alkyl chain on BDT has a great influence on the PCE of the copolymers. In addition, the PCEs of **PHDBDT-T-TR** (3.47%) and **PEHBDT-T-TR** (4.25%) are higher than the analogy polymers **PHDBDT-T-R** (1.01%) and **PEHBDT-T-R** (4.04%) mainly owing to the higher J_{sc} of the former, which shows that the introduction of thienylvinyl unit to extend conjugated side chains is favorable

to improve the J_{sc} and PCE.

One can observe that the best cells based on the four polymers show relatively high V_{oc} values (above 0.85 V), which can be readily understood from their lower-lying HOMO energy levels (Table 2). The highest J_{sc} values of PSCs based on **PEHBDT-T-R** (8.61 mA/cm^2) and **PEHBDT-T-TR** (9.36 mA/cm^2) are higher than those of J_{sc} values based on **PHDBDT-T-R** (3.82 mA/cm^2) and **PHDBDT-T-TR** (7.56 mA/cm^2), which are consistent with the relatively broader absorption spectra and lower bandgaps (Fig. 2 and Table 2). Fig. 7 displays the external quantum efficiency (EQE) curves of the photovoltaic devices under monochromatic light illumination. PSCs based on these polymers exhibit relatively broad EQE responses ranging from 300 to 700 nm with maximum EQE values of 20% at 488 nm, 43% at 460 nm, 46% at 465 nm and 63% at 468 nm for **PHDBDT-T-R**, **PEHBDT-T-R**, **PHDBDT-T-TR** and **PEHBDT-T-TR**, respectively. Compared to the absorption spectra of polymer films (Fig. 2(b)), the broadened EQE responses in the visible region can be attributed to both the intrinsic absorption of the polymers and the response of $PC_{70}BM$. Although the EQE value is not very high, the response covers a reasonable broad spectrum (300-700 nm) and a relatively high EQE value over 50% around 470 nm, which elucidates the obviously higher J_{sc} of **PEHBDT-T-TR**-based cells relative to the other three polymers. Overall, the EQE results are consistent with the J_{sc} values of the corresponding PSCs.

Table 3 Photovoltaic properties of the PSCs based on the four copolymers: $PC_{70}BM$ with different fabricated conditions, under the illumination of AM1.5G, 100 mW/cm^2.

Active layer	DIO	MeOH	V_{oc} (V)	J_{sc} (mA/cm^2)	FF (%)	PCE_{max} (%)[a]	$PCE_{ave.}$ (%)[b]
PHDBDT-T-R:$PC_{70}BM$ =1:1	-	-	0.63	1.00	26.72	0.17	-
PHDBDT-T-R:$PC_{70}BM$ =1:2	-	-	0.68	1.08	33.32	0.25	-
PHDBDT-T-R:$PC_{70}BM$ =1:3	-	-	0.74	2.14	38.66	0.61	-
PHDBDT-T-R:$PC_{70}BM$ =1:3	3%	-	0.65	0.65	29.90	0.13	-

PHDBDT-T-R:$PC_{70}BM$ =1:3	3%	+	0.97	1.77	37.40	0.64	-
PHDBDT-T-R:$PC_{70}BM$ =1:3	-	+	0.82	3.92	32.20	1.01	0.97
PEHBDT-T-R:$PC_{70}BM$ =1:1	-	-	0.69	6.38	35.81	1.58	-
PEHBDT-T-R:$PC_{70}BM$ =1:2	-	-	0.73	7.60	41.80	2.32	-
PEHBDT-T-R:$PC_{70}BM$ =1:2	3%	-	0.87	7.79	48.89	3.31	-
PEHBDT-T-R:$PC_{70}BM$ =1:2	3%	+	0.99	8.61	47.50	4.04	3.89
PEHBDT-T-R:$PC_{70}BM$ =1:2	-	+	0.86	8.14	41.27	2.89	-
PEHBDT-T-R:$PC_{70}BM$ =1:3	-	-	0.69	8.33	38.13	2.19	-
PHDBDT-T-TR:$PC_{70}BM$ =1:1	-	-	0.81	3.75	32.74	1.00	-
PHDBDT-T-TR:$PC_{70}BM$ =1:2	-	-	0.81	4.39	41.09	1.46	-
PHDBDT-T-TR:$PC_{70}BM$ =1:2	3%	-	0.93	3.89	45.33	1.64	-
PHDBDT-T-TR:$PC_{70}BM$ =1:2	3%	+	0.95	7.56	48.31	3.47	3.34
PHDBDT-T-TR:$PC_{70}BM$ =1:2	-	+	0.81	6.07	42.04	2.07	-
PHDBDT-T-TR:$PC_{70}BM$ =1:3	-	-	0.78	3.50	30.59	0.84	-
PEHBDT-T-TR:$PC_{70}BM$ =1:1	-	-	0.69	6.31	46.77	2.04	-
PEHBDT-T-TR:$PC_{70}BM$ =1:1.5	-	-	0.69	7.41	46.20	2.36	-
PEHBDT-T-TR:$PC_{70}BM$ =1:1.5	3%	-	0.69	8.79	46.20	2.80	-
PEHBDT-T-TR:$PC_{70}BM$ =1:1.5	3%	+	0.87	9.36	52.30	4.25	4.01
PEHBDT-T-TR:$PC_{70}BM$ =1:2	-	-	0.66	8.03	40.01	2.12	-

[a]PCE_{max} is the highest PCE of the devices. [b]$PCE_{ave.}$ is the average value of four devices.

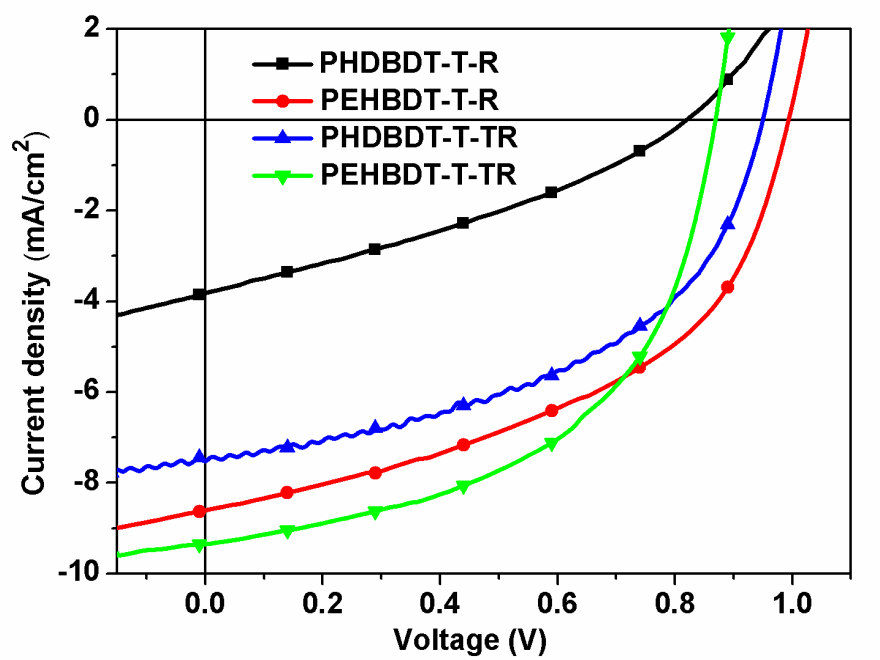

Fig. 6 Typical *J-V* curves of photovoltaic devices based on **PHDBDT-T-R**, **PEHBDT-T-R**, **PHDBDT-T-TR** and **PEHBDT-T-TR** with the best fabricated conditions.

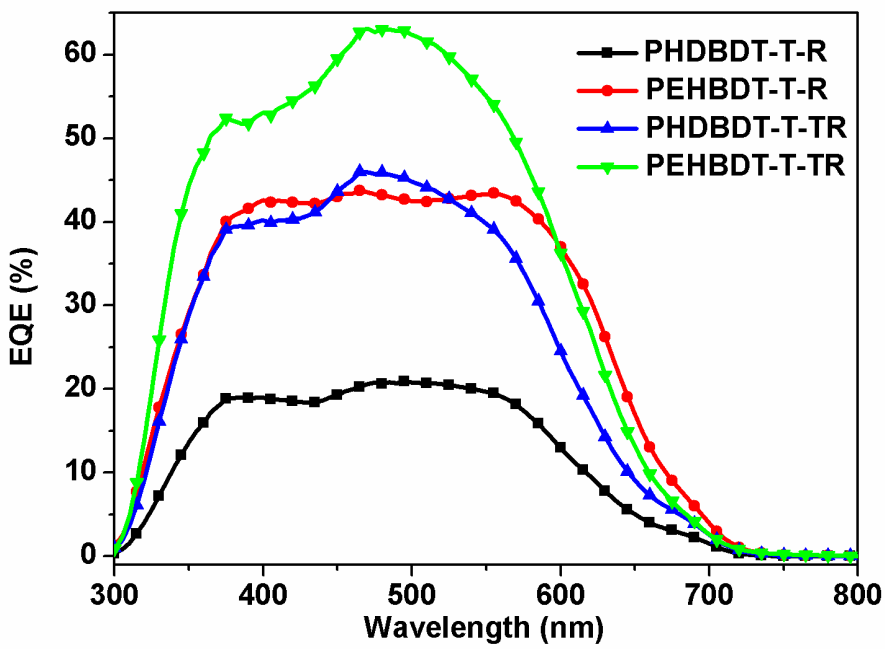

Fig. 7 EQE curves of photovoltaic devices based on **PHDBDT-T-R**, **PEHBDT-T-R**, **PHDBDT-T-TR**, and **PEHBDT-T-TR** with the best fabricated conditions.

Hole Mobility

Hole mobility is an important parameter for the photovoltaic donor materials. Here, hole mobility of the four polymers/$PC_{70}BM$ blend film with the optimal D/A

ratio were measured by using the space-charge-limited current (SCLC) method with the hole-only device structure of ITO/PEDOT:PSS/polymer:$PC_{70}BM$/Au and estimated through the Mott–Gurney equation.[33] For the hole-only devices, SCLC is described by $J = 9\varepsilon_0\varepsilon_r\mu V^2/8L^3\exp[0.891\gamma(V/L)^{0.5}]$, where ε is the dielectric constant of the polymers, ε_0 is the permittivity of the vacuum, μ_0 is the zero-field mobility, E_0 is the characteristic field, J is the current density, and L is the thickness of the film. Fig. 8 shows the $\ln(JL^3/V^2)$ vs $(V/L)^{0.5}$ plots of the polymers measured by the SCLC method. According to the above equation and the curves shown in Fig. 8, the calculated hole mobilities are 1.51×10^{-5} cm^2 V^{-1} s^{-1}, 5.02×10^{-5} cm^2 V^{-1} s^{-1}, 3.04×10^{-5} cm^2 V^{-1} s^{-1}, and 2.75×10^{-4} cm^2 V^{-1} s^{-1} for **PHDBDT-T-R**, **PEHBDT-T-R**, **PHDBDT-T-TR**, and **PEHBDT-T-TR** blend films, respectively. The lower hole mobility of the **PHDBDT-T-R**–based blend film could be related to its lower molecular weight (see Table 1). This should be responsible for its poor photovoltaic performance. On the other hand, **PEHBDT-T-TR**–based blend film showed the highest mobility of all, which could contribute in part to the higher J_{sc} and FF values of the device.

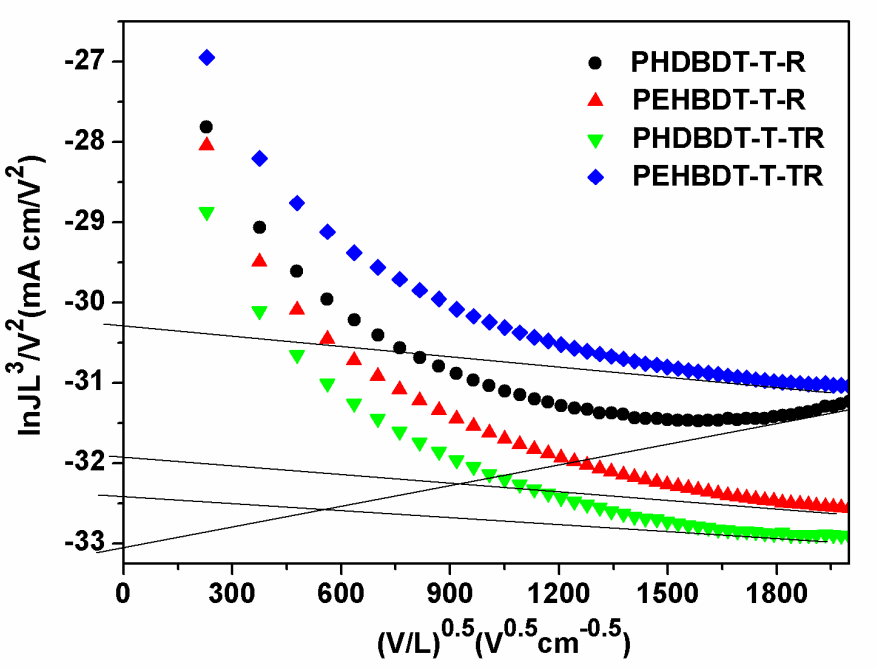

Fig. 8 Plots of $\ln(JL^3\ V^{-2})$ vs $(V^{0.5}L^{-0.5})$ for the measurement of hole mobility in polymer/$PC_{70}BM$ devices by the SCLC method.

Morphological studies

The morphology of the photoactive layer plays an important role in the photovoltaic performance of PSCs along with other photo-physical properties and in several situations the photovoltaic performance of the device strongly depends on its morphological features. To explore the effects of the methanol treatment on the morphology and device performance of polymer/$PC_{70}BM$ film, we observed the surface morphologies of the blend films using atomic force microscopy (AFM). As shown in Fig 9a, when 3 vol % DIO was added, the active layer of **PEHBDT-T-TR** displayed a root-mean-square (RMS) of 3.89 nm. After treating the active layer with methanol, regular columnar domains formed in the phase image, and the surface of the blend film based on **PEHBDT-T-TR** became relatively rough with an increased RMS of 8.07 nm (see Fig. 9b). As some of the polar solvent molecules penetrated the active layer, $PC_{70}BM$ particles redistributed and aggregated to reduce the contact areas with the polar solvents.[34] As a result, solvent-dependent $PC_{70}BM$ migration within the polymer chains enabled the formation of nanoscale phase separation of the blend films (Fig. 9b). This relatively course surface and more ordered structure are beneficial to the charge transportation, thus leading to an increase in J_{sc} and FF as well as the device efficiency. Obviously, the appropriate domain sizes and phase separation can produce the best photovoltaic performance. Furthermore, the similar results can be found from the other three polymers. Figs 9c, d, and e give the AFM height images of the other three polymers after the methanol treatment. It can be seen that the active layers of **PHDBDT-T-R**, **PEHBDT-T-R**, and **PHDBDT-T-TR** displayed RMS of 3.17, 5.31, and 4.60 nm, respectively. Obviously, the active layer of **PEHBDT-T-R** and **PHDBDT-T-TR** show relatively rougher surfaces compared with **PHDBDT-T-R**. In view of the superior photovoltaic performance of **PEHBDT-T-R** and **PHDBDT-T-TR**-based PSCs, the result further suggests that relatively larger phase separation is more favorable for improving the photovoltaic performance.

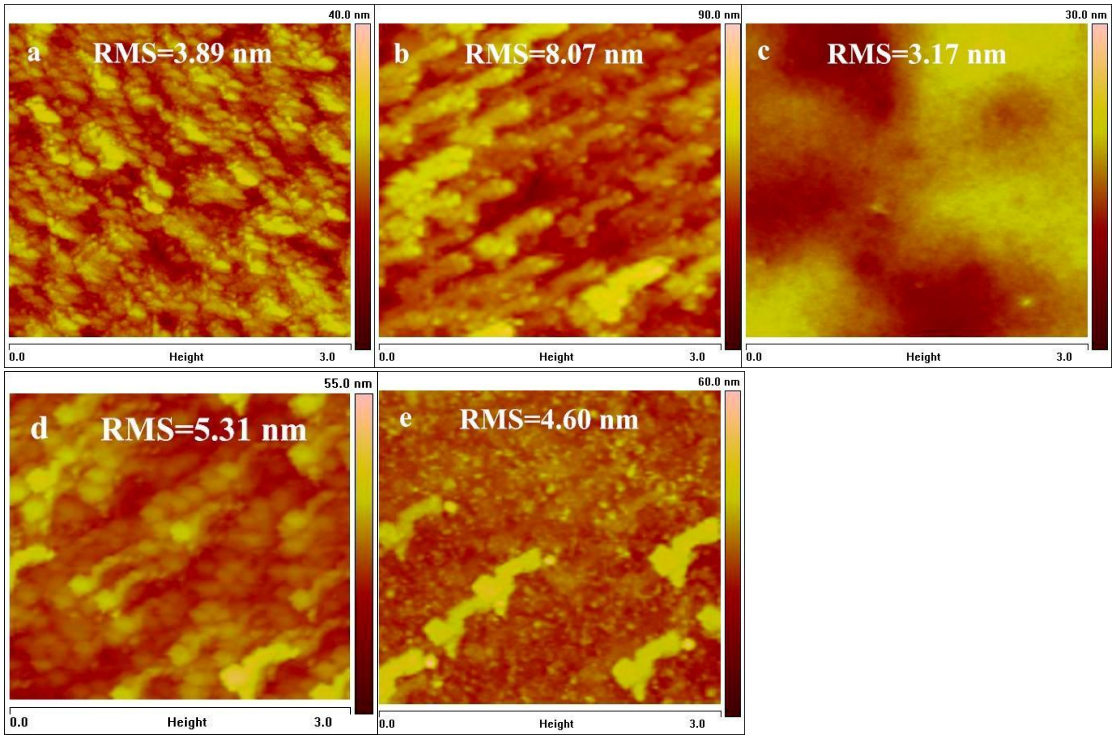

Fig. 9 AFM height images of a **PEHBDT-T-TR**: $PC_{70}BM$(1:1.5, 3 vol % DIO), b **PEHBDT-T-TR**:$PC_{70}BM$(1:1.5, 3 vol % DIO, treated with methanol), c **PHDBDT-T-R**:$PC_{70}BM$ (1:3, treated with methanol), d **PEHBDT-T-R**:$PC_{70}BM$(1:2, 3 vol % DIO, treated with methanol) and e **PHDBDT-T-TR**:$PC_{70}BM$(1:2, 3 vol % DIO, treated with methanol). The imaging size is 3 μm × 3 μm for each panel.

Photoluminescence

In order to gain more insight into the methanol treatment on enhanced efficiency, the PL quenching studies in the presence of $PC_{70}BM$ acceptor were carried out.[27,28,30] We choose **PHDBDT-T-TR** as an example because its PCE changed significantly after treating with methanol (see Table 3). Fig. 10 gives the PL spectra of the pristine **PHDBDT-T-TR**, **PHDBDT-T-TR**:$PC_{70}BM$ (3 vol % DIO) with and without methanol treatment. The pristine **PHDBDT-T-TR** displays the emission in the range of 600−800 nm with a peak at 671 nm. Upon blending **PHDBDT-T-TR** with $PC_{70}BM$, the PL is significantly quenched as shown in Fig. 10. The PL is further quenched after treating the **PHDBDT-T-TR**:$PC_{70}BM$ blend film with methanol. This effective PL quenching suggests that the exciton separation is highly efficient in polymer:$PC_{70}BM$ blend films. The more effective quenching in the **PHDBDT-T-TR**:$PC_{70}BM$ blend

with methanol treatment than that without treatment implies that the feasibility of exciton dissociation process in polymer:$PC_{70}BM$ blend film is increased further after the methanol treatment. Therefore, the PL quenching studies reveal that the polymer:$PC_{70}BM$ blend film with methanol treatment has more favorable features for the higher J_{sc}.

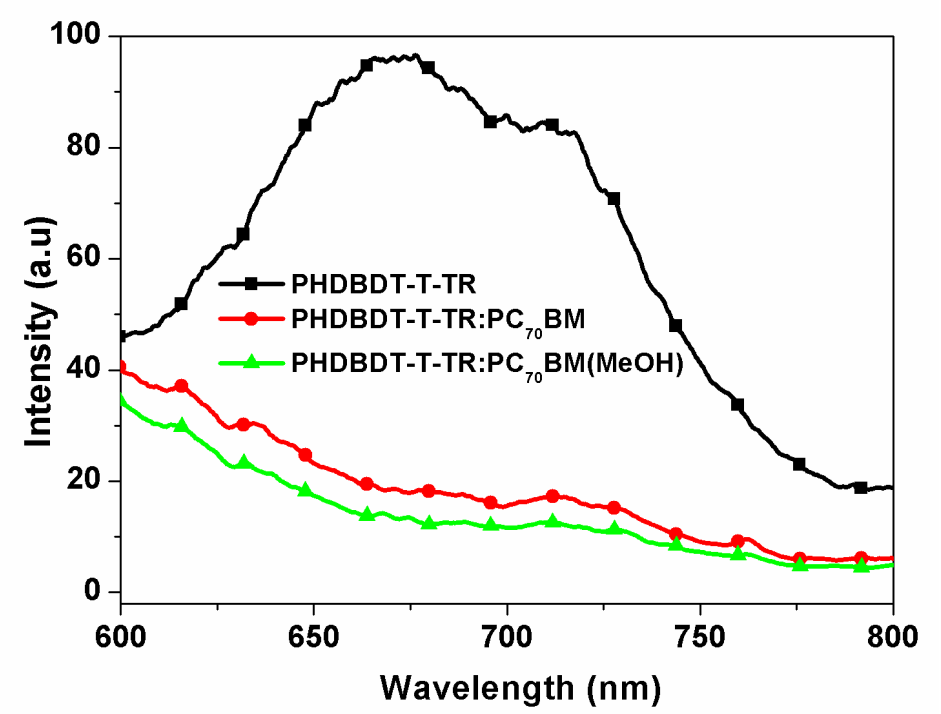

Fig. 10 Photoluminescence spectra of pristine **PHDBDT-T-TR**, **PHDBDT-T-TR**: $PC_{70}BM$ (3 vol % DIO) without and with methanol treatment.

Conclusions

Four main chain-side chain D-A copolymers, **PHDBDT-T-R**, **PEHBDT-T-R**, **PHDBDT-T-TR**, and **PEHBDT-T-TR** containing the same backbone of alternative BDT-thiophene but different side chains bearing on BDT and thiophene units were designed, synthesized and utilized for BHJ PSCs. We found that the type and shape of the side chains have great influences on the solubility, light absorption, HOMO/LUMO energy levels, and charge transport properties of the resulting polymers as well as morphology and photovoltaic properties of the PSCs. Optical and electrochemical properties showed that the introduction of thienylvinyl unit between the thiophene and 3-ethylrhodanine as conjugated side chains can slightly reduce

bandgaps and elevate HOMO levels of the polymers. The BHJ PSCs based on four polymers were prepared and the device fabrication conditions, including the different blend ratio of the polymer donor and acceptor, the additive of 1, 8-diiodooctane (DIO) and methanol treatment, have been optimized in detail. The effects of methanol treatment on the enhancement in photovoltaic performance especially for the J_{sc} and FF of the PSCs are demonstrated to originate from the increased exciton separation efficiency, charge carrier mobilities and the formation of fiber-like interpenetrating network morphologies. After systematically optimizing, the best PCEs were improved up to 1.01%, 4.04%, 3.47%, and 4.25% for **PHDBDT-T-R**, **PEHBDT-T-R**, **PHDBDT-T-TR**, and **PEHBDT-T-TR**, respectively, mainly due to significantly increased J_{sc} and FF. This work could provide some insight into side chain engineering to efficiently construct photovoltaic polymers.

Experiment section

Measurements and characterization

Solvents were dried and distilled from appropriate drying agents prior to use. Commercially available reagents were used without further purification. ^{1}H NMR spectra and ^{13}C NMR spectra were measured on a Bruker DMX−400 spectrometer with $CDCl_3$ as the solvent and $(CH_3)_3SiH$ as the internal reference. Mass spectra (MS) were recorded on a Shimadzu spectrometer and MALDI-TOF-MS spectra were determined on a Bruker BIFLEX III mass spectrometer. Molecular weights of the polymers were measured by gel permeation chromatography (GPC) with polystyrenes as standard and chloroform ($CHCl_3$) as an eluent. UV−vis absorption spectra were obtained on a Hitachi U-3010 UV−vis spectrophotometer. Thermogravimetric analysis (TGA) was conducted on a Perkin−Elmer TGA−7 thermogravimetric analyzer at a heating rate of 10 ℃/min and under a nitrogen flow rate of 100 mL/min. The electrochemical cyclic voltammetry (CV) was performed on a Zahner IM6e Electrochemical Workstation, with a glassy carbon disc coated with polymer film as the working electrode, Pt wire as the counter electrode and Ag/AgCl electrode as the reference electrode, respectively, in a 0.1 mol/L Bu_4NPF_6 acetonitrile solution at a

scan rate of 100 mV/s. The morphology of blend films was measured using an atomic force microscope (AFM, Digital Instrument Multimode Nanoscope IIIA) using the tapping mode.

PSCs Device fabrication and characterization

PSCs were fabricated with ITO glass as a positive electrode, Ca/Al as a negative electrode and the blend film of polymer/$PC_{70}BM$ between them as a photosensitive layer. The patterned ITO glass was precleaned by ultrasonication with detergent water, deionized water, acetone and isopropanol each for 20 min, then treated in an ultraviolet-ozone chamber (Jelight Co.) for 20 min. A thin layer of PEDOT:PSS (poly(3, 4-ethylenedioxythiophene):poly(styrenesulfonate)) was spin-cast on precleaned ITO-coated glass from a PEDOT:PSS aqueous solution (Clevious P VP AI 4083 H. C. Stark, Germany) at 3000 rpm for 40 s and dried subsequently at 150 ℃ for 15 min in air, and the thickness of the PEDOT:PSS layer is about 40 nm. After that, transfer the device to the glovebox. The photosensitive layers, a blend solution of the polymer and $PC_{70}BM$ with the poly concentration of 13.3 mg/mL in 1, *2*-dichlorobenzene (DCB) was spin-coated on ITO/PEDOT:PSS electrode. Finally, the Ca/Al cathode was deposited in vacuum on the active layer under the pressure of ca. 9×10^{-5} Pa. The active area of the investigated device was 5 mm^2. The current density−voltage (*J*−*V*) characteristics were conducted on a computer-controlled Keithley 236 Source−Measure Unit in a dry box under an inert atmosphere. A xenon lamp (150 W) coupled with AM 1.5 solar spectrum filter was used as the white light source, and the optical power at the sample was 100 mW/cm^2. The external quantum efficiency (EQE) was measured by a Stanford Research Systems model SR830 DSP lock-in amplifier coupled with a WDG3 monochromator and a 500W xenon lamp. The light intensity at each wavelength was calibrated with a standard single-crystal Si photovoltaic cell. The hole mobility was calculated by fitting the dark *J*−*V* curves for the hole-only devices to SCLC model at low voltages, in which the current density is given by $J = 9\varepsilon_0\varepsilon_r\mu V^2/8L^3\exp[0.891\gamma(V/L)^{0.5}]$, where $\varepsilon_0\varepsilon_r$ represents the permittivity of the material, μ is the mobility, γ is the field activation factor, and L the thickness of

the active layer. The applied bias voltage is corrected for the built-in potential so that $V = V_{applied} - V_{bi}$.

Materials

N-Bromosuccinimide (NBS), thiophene-3-carbaldehyde, thiophene-2-carbaldehyde, 3-methylthiophene, 3-ethylrhodanine, *t*-BuOK, and $Pd(PPh_3)_4$ were purchased from J&K Chemical or Alfa Aesar. Toluene, DMF, THF, $POCl_3$ and $ClCH_2CH_2Cl$ were carefully dried and distilled prior to use. All other reagents and solvents used in this work were commercially purchased and used without further purification. 2,5-Bibromo-3-(bromomethyl)thiophene, 2,5-dibromo-3-methylthiophene, (2,5-dibromothiophen-3-ylmethyl)phosphonic acid diethyl ester[28] and **M3**, **M4** were synthesized by the reported procedures.[19] The detailed synthetic procedures of other compounds are as follows.

Synthesis of the monomers and polymers

2, 5-Dibromothiophene-3-carbaldehyde (1). Thiophene-3-carbaldehyde (2.24 g, 20mmol) was placed in a 100mL round-bottom flask and added a bit of DMF to dissolve. Then NBS (7.48 g, 42 mmol) was dissolved in an appropriate amount of anhydrous DMF. The mixture was added dropwise to the flask in the dark. The resulting solution was stirred at room temperature all day. Then, the mixture was extracted with dichloromethane, the organic layer was washed with water and dried over anhydrous $MgSO_4$, and the solvent was removed under vacuum. After that, the crude product was purified through the silica gel column with a petroleum ether/dichloromethane mixture (4:1 by volume) as eluent. A creamy yellow solid was obtained. Yield: 3.61 g (67%).^{1}H NMR (400 MHz, $CDCl_3$, δ/ppm): 9.82 (s, 1H), 7.36 (s, 1H). ^{13}C NMR (100 MHz, $CDCl_3$, δ/ppm): 183.0, 139.4, 128.7, 124.0, 113.3. MS (EI): m/z: calcd for $C_5H_2Br_2OS$: 269.9; found: 269.5.

(*Z*)-5-((2,5-Dibromothiophen-3-yl)methylene)-3-ethyl-2-thioxothiazolidin-4-one (M1). The **Monomer 1** was synthesized by the Knoevenagel reaction. Compound 1 (2.70 g, 10.0 mmol), 3-ethylrhodanine (1.62 g, 10.0 mmol) and 30 mL $CHCl_3$ was added in a 50 mL dual-mouth flask under argon protection. Subsequently, 0.5 mL

piperidine was injected into the reaction mixture, and then the mixture was heated reflux overnight. Then cooling to ambient temperature, the mixture was extracted by chloroform, and the combined organic phase was washed with water several times, dried over $MgSO_4$. After that, the crude product was purified through the silica gel column with a petroleum ether/dichloromethane mixture (2:1 by volume) as eluent to give **Monomer 1** as a yellow solid. Yield: 2.9 g (70%). ^{1}H NMR (400 MHz, $CDCl_3$, δ/ppm): 7.59 (s, 1H), 7.13 (s, 1H), 4.21-4.15 (m, 2H), 1.286 (t, 3H, J = 7.2 Hz). ^{13}C NMR (100 MHz, $CDCl_3$, δ/ppm): 206.9, 191.5, 167.3, 135.4, 128.1, 124.6, 123.1, 119.9, 113.7, 39.9, 30.9, 12.2. MS (EI): m/z: calcd for $C_{10}H_7Br_2NOS_3$: 413.2; found: 413.2

(*E*)-2,5-Dibromo-3-(2-(thiophen-2-yl)vinyl)thiophene (2). (2,5-Dibromothiophen-3-ylmethyl)phosphonic acid diethyl ester (6.28 g, 14.9 mmol) and thiophene-2-carbaldehyde (1.67 g, 14.9 mmol) were dissolved in THF (20 mL) and the solution was stirred at room temperature for 30 min under argon atmosphere. Then *t*-BuOK (1.94 g, 17.14 mmol) was dissolved in THF (20 mL) and added dropwise to the solution. The reaction mixture was stirred at room temperature for 5 h, and then heated to 50 ℃ reflux for 12 h. After cooling to room temperature, the reaction mixture was poured into dilute aqueous HCl (20 mL) solution and extracted with dichloromethane. The organic layer was washed with water and dried over anhydrous $MgSO_4$, and then the solvent was removed by rotary evaporation. The crude product was purified by column chromatography on silica gel using petroleum ether as eluent to afford compound **2** as a yellow solid. Yield: 3.68 g (70%). ^{1}H NMR (400 MHz, $CDCl_3$, δ/ppm): 7.22 (s, 1H), 7.08 (s, 1H), 7.05 (s, 1H), 7.00 (d, 2H, J = 12.0 Hz), 6.81 (s, 1H). ^{13}C NMR (100 MHz, $CDCl_3$, δ/ppm): 141.8, 138.7, 127.7, 127.1, 126.7, 125.1, 124.2, 119.4, 111.8, 109.7. MS (EI): m/z: calcd for $C_{10}H_6Br_2S_2$: 350.1; found: 350.2

(*E*)-5-(2-(2, 5-Dibromothiophen-3-yl)vinyl)thiophene-2-carbaldehyde (3). The compound 3 was synthesized by the Vilsmeier reaction. To the mixture of compound 2 (3.4 g, 9.7 mmol) in 1, 2-dichloroethane (25 mL) and anhydrous DMF (0.71 mL, 9.7 mmol) was added dropwise under argon atmosphere, then $POCl_3$ (0.85 mL, 9.7 mmol)

was added slowly. The mixture was stirred at 85 ℃ for 12 h. Then cooled the mixture to room temperature, added 30 mL saturated sodium acetate solution to the mixture, stirred 70 min at the room temperature. After that, 30 mL of water was added to quench the reaction. The mixture was extracted with CH_2Cl_2, the combined the organic phase was washed with water 3 times and dried over anhydrous $MgSO_4$, and then the solvent was removed under vacuum. The crude product was purified on silica gel chromatography using a petroleum ether/dichloromethane mixture (4:1 by volume) as eluent. A yellow powder was obtained. Yield: 2.39 g (65%). ^{1}H NMR (400 MHz, $CDCl_3$, δ/ppm): 9.87 (s, 1H), 7.66 (d, 1H, J = 3.6 Hz), 7.18 (t, 2H, J = 5.6 Hz), 7.02 (d, 2H, J = 2.0 Hz). ^{13}C NMR (100 MHz, $CDCl_3$, δ/ppm): 182.3, 156.0, 142.0, 137.7, 136.7, 126.9, 126.8, 123.4, 122.9, 112.3, 112.2. MS (EI): m/z: calcd for $C_{11}H_6Br_2OS_2$: 378.1; found: 378.1

(Z)-5-((5-((*E*)-2-(2,5-Dibromothiophen-3-yl)vinyl)thiophen-2-yl)methylene)-3-ethyl-2-thioxothiazolidin-4-one (M2). By following the similar method used for **M1**, **M2** was synthesized with compound 3 (1.5 g, 3.96 mmol) and 3-ethylrhodanine (0.638 g, 3.96 mmol). The final product was obtained as a red solid. Yield: 1.48 g (72%). ^{1}H NMR(400 MHz, $CDCl_3$, δ/ppm): 7.82 (s, 1H), 7.31 (d, 1H, J = 4.0 Hz), 7.17 (s, 1H), 7.13 (d, 1H, J = 4.0 Hz), 7.03 (s, 1H), 7.01-6.92 (m, 1H), 4.19 (d, 2H, J = 7.2 Hz), 0.89 (t, 3H, J = 2.4 Hz). ^{13}C NMR (100 MHz, $CDCl_3$, δ/ppm): 192.0, 167.3, 149.8, 149.8, 138.2, 137.3, 135.0, 128.3, 127.1, 124.9, 123.2, 122.4, 112.5, 112.0, 40.0, 12.3. MALDI-TOF: MS (EI): m/z: calcd for $C_{16}H_{11}Br_2NOS_4$: 521.3; found: 521.2.

PHDBDT-T-R. The polymerization was performed by a Stille coupling reaction. In a 50 mL flask, **M1** (123 mg, 0.30 mmol) and **M3** (299 mg, 0.30 mmol) were dissolved in 10 mL toluene, and the solution was flushed with argon for 15 min, then 50 mg $Pd(PPh_3)_4$ was added into the solution. The mixture was again flushed with argon for 20 min. The reaction mixture was heated to reflux for 24 h. The reaction mixture was cooled to room temperature and added dropwise to 200 mL methanol. The precipitate was collected and further purified by Soxhlet extraction with methanol, hexane, in sequence. The hexane fraction was concentrated and added dropwise into

methanol. Finally, the precipitates were collected and dried under vacuum overnight to get **PHDBDT-T-R** as a black red solid (114 mg, yield 41.6%). ^{1}H NMR (400 MHz, $CDCl_3$, δ/ppm): 8.22 (br, 1H), 8.06 (br, 1H), 7.88 (br, 1H), 7.67 (br, 1H), 4.58-3.84 (m, 6H), 2.20-1.96 (m, 2H), 1.33-0.89 (m, 63H).

PEHBDT-T-R. PEHBDT-T-R was synthesized by following the same procedure for **PHDBDT-T-R**. **M1** (123 mg, 0.30 mmol) and **M4** (232 mg, 0.30 mmol) were used as starting materials. Finally, **PEHBDT-T-R** was obtained as a dark-red solid (163 mg, yield 78.3%). ^{1}H NMR (400 MHz, $CDCl_3$, δ/ppm): 8.22 (br, 1H), 8.06 (br, 1H), 7.88 (br, 1H), 7.67 (br, 1H), 4.58-3.84 (m, 6H), 2.20-1.96 (m, 2H), 1.37-0.99 (m, 31H).

PHDBDT-T-TR. PHDBDT-T-TR was synthesized by following the same procedure for **PHDBDT-T-R**. **M2** (156 mg, 0.30 mmol) and **M3** (299 mg, 0.30 mmol) were used as starting materials. But the precipitate was collected and further purified by Soxhlet extraction with methanol, hexane, chloroform in sequence. The chloroform fraction was concentrated and added dropwise into methanol. Finally, **PHDBDT-T-TR** was obtained as a dark-red solid (157 mg, yield 51.1%). ^{1}H NMR (400 MHz, $CDCl_3$, δ/ppm): 7.84 (br, 1H), 7.55 (br, 1H), 7.52 (br, 1H), 7.49 (br, 1H), 7.38 (br, 1H), 7.21 (br, 1H), 7.17 (br, 1H), 6.99 (br, 1H), 4.25-3.80 (m, 6H), 1.95-1.83 (m, 2H), 1.26-0.82 (m, 63H).

PEHBDT-T-TR. PEHBDT-T-TR was synthesized by following the same procedure for **PEHBDT-T-R**. **M2** (130 mg, 0.25 mmol) and **M4** (193 mg, 0.25 mmol) were used as starting materials. Finally, **PEHBDT-T-TR** was obtained as a dark-red solid (146 mg, yield 72.6%). ^{1}H NMR (400 MHz, $CDCl_3$, δ/ppm): 7.84 (br, 1H), 7.55 (br, 1H), 7.52(br, 1H), 7.48 (br, 1H), 7.37 (br, 1H), 7.20 (br, 1H), 7.17 (br, 1H), 7.00 (br, 1H), 4.25-3.80 (m, 6H), 1.94-1.82 (m, 2H), 1.26-0.89 (m, 31H).

Acknowledgements

This work was supported by the Natural Science Foundation of Hunan Province, China (Grant No. 2015JJ3019) and the Key Research Foundation of Education Bureau of Hunan Province, China (Grant No. 14A147).

References

1 L. Ye, S. Zhang and J. Hou, *Acc. Chem. Res.*, 2014, **47**, 1595–1603.

2 Y. Liu, J. Zhao, Z. Li, C. Mu, W. Ma, H. Hu, K. Jiang, H. Lin, H. Ade and H. Yan, *Nat. Commun.*, 2014, **5**, 5293–5300.

3 Z. He, B. Xiao, F. Liu, H. Wu, Y. Yang, S. Xiao, C. Wang, T. P. Russell and Y. Cao, *Nat. Photonics.*, 2015, **9**, 174–179.

4 J. You, L. Dou, K. Yoshimura, T. Kato, K. Ohya, T. Moriarty, K. Emery, C.-C. Chen, J. Gao, G. Li and Y. Yang, *Nat. Commun.*, 2013, **4**, 1446–1455.

5 Y. Li, *Acc. Chem. Res.*, 2012, **45**, 723–733.

6 G. Yu, J. Gao, J. C. Hummelen, F. Wudl and A. J. Heeger, *Science*, 1995, **270**, 1789–1791.

7 L. Ye, S. Zhang and J. Hou, *Acc Chem. Res.*, 2014, **47**, 1595–1603.

8 C. Cui, W. Wong and Y. Li, *Energy Environ. Sci.*, 2014, **7**, 2276–2284.

9 M. Zhang, X. Guo, S. Zhang and J. Hou, *Adv. Mater.*, 2014, **26**, 1118–1123.

10 J. Zhou, X. Wan, Y. Liu, Y. Zuo, Z. Li, G. He, G. Long, W. Ni, C. Li, X. Su and Y. Chen, *J. Am. Chem. Soc.*, 2012, **134**, 16345–16351.

11 P. Shen, H. Bin, X. Chen, Y. Li, *Org. Electron.*, 2013, **14**, 3152–3162.

12 M. Wang, D. Ma, K. Shi, S. Shi, S. Chen, C. Huang, Z. Qiao, Z. Zhang, Y. Li, X. Li and H. Wang, *J. Mater. Chem. A*, 2015, **3**, 2802–2814.

13 G. Li, Z. Lu, C. Li and Z. Bo, *Polym. Chem.*, 2015, **6**, 1613–1618.

14 O. Dan, M. Xiao, D. Zhu, W. Zhu, Z. Du, N. Wang, Y. Zhou, X. Bao and R. Yang, *Polym. Chem.*, 2015, **6**, 55–63.

15 T. Lei, J.-Y. Wang and J. Pei, *Chem. Mater.*, 2014, **26**, 594–603.

16 Z.-G. Zhang and Y. Li, *Sci. China Chem.*, 2015, **58**, 192–209.

17 L.Ye, S. Zhang, W. Zhao, H. Yao and J. Hou, *Chem. Mater.*, 2014, **26**, 3603–3605.

18 S. Q. Zhang, L. Ye, W. C. Zhao, B. Yang, Q. Wang, J. H. Hou,.*Sci China Chem*, 2015, **58**, 248–256.

19 J. Hou, H. Chen, S. Zhang, R. Chen, Y. Yang, Y. Wu and G. Li, *J. Am. Chem. Soc.*, 2009, **131**, 15586–15587.

20 J. Hou, L. Huo, C. He, C. Yang and Y Li, *Macromolecule*s, 2006, **39**, 594–603.

21 Z. Gu, P. Shen, S.-W. Tsang, Y. Tao, B. Zhao, P. Tang, Y. Nie, Y. Fang and S. Tan, *Chem. Commun.*, 2011, 47, 9381–9383.

22 S. C. Price, A. C. Stuart and W. You, *Macromolecules*, 2010, **43**, 4609–4612.

23 B. C. Thompson, Y. G. Kim and J. R. Reynolds, *Macromolecules*, 2005, **38**, 5359.

24 M. C. Scharber, D. Muhbacher, M. Koppe, P. Denk, C. Waldauf, A. J. Heeger and C. J. Brabec, *Adv. Mater.*, 2006, **18**, 789–794.

25 Y. He and Y. Li, *Phys. Chem. Chem. Phys.*, 2011, **13**, 1970–1983.

26 X. Liu, W. Wen and G. C. Bazan, *Adv. Mater.*, 2012, **24**, 4505–4510.

27 Y. Wang, Y. Liu, S. Chen, R. Peng and Z. Ge, *Chem. Mater.*, 2013, **25**, 3196–3204.

28 P. Shen, H. Bin, L. Xiao and Y. Li, *Macromolecules*, 2013, **46**, 9575–9586.

29 S. Nam, J. Jang, H. Cha, J. Hwang, T. K. An, S. Park and C. E. Park, *J. Mater. Chem.*, 2012, **22**, 5543–5549.

30 K. Kranthiraja, K. Gunasekar, W. Cho, M. Song, Y. G. Park, J. Y. Lee, Y. Shin, I.-N. Kang, A. Kim, H. Kim, B. Kim and S.-H. Jin, *Macromolecules*, 2014, **47**, 7060–7069.

31 K. Kranthiraja, K. Gunasekar, W. Cho, Y.G. Park, J.Y. Lee, Y. Shin, I.-N. Kang, M. Song, K. H. Chae, B. Kimef and S.-H. Jin, *J. Mater. Chem. C*, 2015, **3**, 796–808.

32 B. Qi and J. Wang, *J. Mater. Chem.*, 2012, **22**, 24315–24325.

33 T. Y. Chu and O. K. Song, *Appl. Phys. Lett.*, 2007, **90**, 203512–203513.

34 S. Nam, D. S. Chung, J. Jang, S. H. Kim, C. Yang, S.-K. Kwon and C. E. Park, *J. Electrochem. Soc.*, 2010, **157**, H90–H93.

A table of contents

Four benzodithiophene-thiophene copolymers with conjugated side chain containing electron-withdrawing ethylrhodanine acceptor unit were designed and synthesized. The PSCs based on the four polymers showed the highest PCE of 4.25%.